On discrete boundaries and solution accuracy in anisotropic adaptive meshing

Konstantin Lipnikov[1] and Yuri Vassilevski[2]

[1] Los Alamos National Laboratory, lipnikov@lanl.gov
[2] Institute of Numerical Mathematics, vasilevs@dodo.inm.ras.ru

1 Introduction

Large-scale simulations in engineering applications are most effective when they are combined with adaptive methods. The adaptive methods reduce greatly the demand for larger number of unknowns and improve accuracy of the simulations via grid adaptation near fine-scale features of the solution. In this paper, we consider a tensor metric based adaptive methodology [AG99, HE98, BU97, HA95, LI03, VA03]. The metric is induced by an approximate Hessian (matrix of second derivatives) of a discrete solution. The focus of this paper is on treatment of curved (non-planar) internal and boundary surfaces.

In many applications, exact parameterization of curved surfaces may be unknown. In this case, the surfaces are described by triangular meshes (e.g., meshes coming from CAD systems) which reduce performance of adaptive methods due to the limited surface resolution. To resolve geometrical features of a model, the trace of an optimal adaptive mesh on a curved surface should be close to the given surface triangulation which is not always the case. One of the possible solutions is to fix only nodes of the surface triangulation (see [VA05] for a more adequate solution) which imposes simple constraints for mesh adaptation algorithms. The fixed-node constraints are easily embedded into the metric-based adaptive methodology.

If the underlying surfaces are sufficiently smooth (or piecewise smooth), the original triangular meshes carry additional information about these surfaces. In this paper, we use this fact to design a new surface reconstruction method and analyze it both theoretically and numerically. In principle, the reconstructed surface can be triangulated to use again the metric-based adaptive methodology with the fixed-node constraints.

There are many methods for higher order reconstruction of piecewise linear surfaces (see [GA05, MI97, ME02, MO01] and references therein). In [MI97, MO01] the surface is parameterized and the desired surface characteristics are computed from the derivatives of functions specifying the parameterization. In [GA05, MI97], the discrete surface is approximated by a piecewise quadratic surface using the best fit algorithm. The method proposed in this paper uses technique of the discrete differential geometry to compute an approximate Hessian of a piecewise quadratic function representing the reconstructed surface. The Hessian is computed in a weak

sense by analogy with the finite element methods. The developed method is exact for quadratic surfaces.

The reconstruction method is local, and therefore it can be easily parallelized. Its computational cost is proportional to the number of surface triangles.

We demonstrate efficiency of the reconstruction method for the solution of a convection-diffusion problem simulating transport phenomena around a spherical obstacle. The solution has a boundary layer along a part of the obstacle boundary. As the result, accuracy of the discrete solution depends on the accuracy of the boundary representation and is significantly improved on the reconstructed surfaces.

The paper outline is as follows. In Section 2, we describe briefly the Hessian based adaptation methodology. In Section 3, we propose and analyze a new surface reconstruction method. In Section 4, we illustrate our adaptive methodology with numerical tests.

2 Hessian Based Mesh Adaptation

2.1 Quasi-Optimal Meshes

Let Ω_h be a mesh with $N(\Omega_h)$ elements and u_h be a discrete piecewise linear solution computed at mesh nodes with some numerical method which we denote by $\mathcal{P}_{\Omega_h}$. We shall simply write that $u_h = \mathcal{P}_{\Omega_h} u$ where u is an unknown exact solution. The ideal goal would be to find a mesh (probably anisotropic) which minimizes the maximal norm of the discretization error $\|u - \mathcal{P}_{\Omega_h} u\|_\infty$. In many problems, this error can be majorized by the interpolation error, $\|u - \mathcal{I}_{\Omega_h} u\|_\infty$, where $\mathcal{I}_{\Omega_h}$ is the linear interpolation operator on mesh Ω_h. It gives us the following mesh optimization problem:

$$\Omega_h^{opt} = \arg \min_{N(\Omega_h) < N_{\max}} \|u - \mathcal{I}_{\Omega_h} u\|_\infty \tag{1}$$

where $N_{\max}$ is the maximal number of mesh elements (tetrahedra) defined by the user. This problem was analyzed both theoretically and numerically in [AG99, VA03]. In fact, problem (1) was replaced by a simpler problem which provides a constructive way for finding an approximate solution of (1) which we refer to as a *quasi-optimal* mesh. This mesh is quasi-uniform in the metric $|H^h|$ derived from the discrete Hessian H^h of u_h. The generation of quasi-uniform meshes is based on the notion of a *mesh quality*.

Let G be a metric generated by a symmetric positive definite 3×3 matrix whose entries depend on point $\mathbf{x} \in \Omega$. For an element e in Ω_h, we denote by $|e|_G$ its volume in metric G and by $|\partial\partial e|_G$ the total length of its edges (also in metric G). We define the mesh quality as

$$Q(\Omega_h) = \min_{e \in \Omega_h} Q(e) \tag{2}$$

where $Q(e)$ is the quality of a single element e,

$$Q(e) = 6\sqrt[4]{2} \frac{|e|_G}{|\partial\partial\, e|_G^3} F\left(\frac{|\partial\partial\, e|_G}{6h^*}\right), \; 0 < Q(e) \leqslant 1. \tag{3}$$

Here h^* is the mesh size in the G-uniform mesh with N_{max} elements and $F(t)$ is a continuous smooth function, $0 \leqslant F(t) \leqslant 1$, with the only maximum at point 1,

$F(1) = 1$, and such that $F(0) = F(+\infty) = 0$. The last factor in (3) controls the size of the element, whereas the remaining factors control its shape.

The optimization of the mesh Ω_h with respect to the mesh quality (2) results in a G-quasi-uniform grid. Since the mesh quality is as good as the quality of the worst element, the mesh optimization can be achieved with a series of *local* operations applied to this element. The list of such operations includes alternation of topology with node deletion/insertion, edge/face swapping and node movement (see Fig. 1 for 2D analogs of local operations and [AG99] for more details).

The local operations such as node deletion/insertion and edge/face swapping are well described in the literature while implementation of the node movement requires additional comments. It is driven by minimization of the smooth functional $\mathcal{F} : \mathbb{R}^3 \to \mathbb{R}$, of the node position $\mathbf{x}$, defined as a reciprocal of the mesh quality (2), i.e. $1 \leqslant \mathcal{F} < \infty$. Some restrictions have to be imposed on mesh modifications to keep the mesh unfolded and to preserve internal and boundary surfaces.

2.2 Adaptive Iterative Algorithm

We use the following loop to build a quasi-optimal mesh:

- Generate any initial tetrahedrization $\Omega_h^{(1)}$ of the computational domain.
- For $k = 1, 2, \ldots$, repeat
  - Compute the discrete solution u_h and generate the discrete Hessian-based metric $|H^h|$ which is the symmetric positive definite matrix given by

$$H^h = W_h \Lambda_h W_h^T, \quad |H^h| = W_h |\Lambda_h| W_h^T$$

    where W_h is the orthonormal matrix, $\Lambda_h = \mathrm{diag}\{\lambda_1, \lambda_2, \lambda_3\}$ is the diagonal matrix, and

$$|\Lambda_h| = \mathrm{diag}\{\max\{|\lambda_1|; \varepsilon\}, \max\{|\lambda_2|; \varepsilon\}, \max\{|\lambda_3|; \varepsilon\}\}$$

    with $\varepsilon > 0$ being a user defined tolerance.
  - Terminate the adaptive loop if the mesh quality in metric $|H^h|$ is bigger than Q_0 which is the user defined number (e.g., $Q_0 \sim 0.4$).
  - Generate the mesh $\Omega_h^{(k+1)}$ which is quasi-uniform in the metric $|H^h|$ and is such that $Q(\Omega_h^{(k+1)}) > Q_0$. To do this, we use local operations such as node deletion/insertion, edge/face swapping and node movement (see Fig. 1).

It is proved in [AG99] that quasi-optimal meshes in polyhedral domains result in the asymptotically optimal estimate:

$$\|u - \mathcal{I}_{\Omega_h} u\|_\infty \sim N(\Omega_h)^{-2/3}. \tag{4}$$

In Section 3, we demonstrate numerically that (4) holds in a more general case of curved boundaries. We also show that the optimal estimate is violated when these boundaries are represented by triangular meshes.

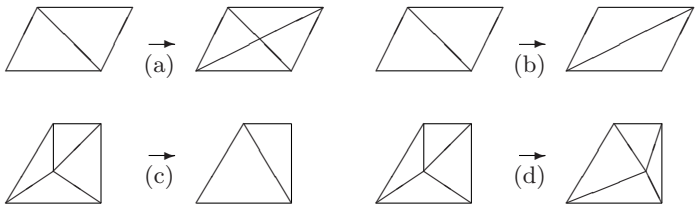

Fig. 1. Local topological operations for 2D triangular meshes: (a) node insertion, (b) edge swapping, (c) node deletion, and (d) node movement

2.3 Treatment of Surface Constraints

The distinctive geometrical features of any model are internal and boundary surfaces (*feature surfaces*) and their intersections (*feature edges*). Let us consider a particular feature surface $\Gamma \subset \mathbb{R}^3$ and a feature edge $\Theta \subset \mathbb{R}^3$. If the analytical formulae for Γ and Θ were available, they could be used in the metric-based adaptive methodology. For example, a node living on the feature surface could be easily projected on the analytic surface.

Often, the analytic representation may not be available for all geometric features constituting the model. In this case, the geometric features are modeled with faces and edges of the original mesh $\Omega_h^{(1)}$. It is highly desirable if the trace of the quasi-optimal mesh on a geometric feature is close to the given feature triangulation. One of the possible solutions is discussed below.

Let the discrete feature surface Γ_h be the triangulated surface of the original mesh ${\Omega_h}^{(1)}$ approximating Γ with triangular faces Γ_t, $\Gamma_h = \cup_t \Gamma_t$, and the discrete feature edge Θ_h be a polyline formed by the edges of ${\Omega_h}^{(1)}$ approximating Θ. In this paper, we fix (freeze) nodes living on Γ_h and Θ_h. This imposes simple constraints on the local mesh modifications and leaves enough freedom for realization of mesh modifications with surrounding tetrahedra. Still, the fixed-nodes constraints may result in unnecessary fine mesh in domains where solution u_h is very smooth. The more adequate treatment of discrete boundaries is described in [VA05].

In Section 5, we shall demonstrate that accuracy of boundary representation makes significant impact on accuracy of the discrete solution. The accuracy may be improved if we assume that the underlying surfaces are sufficiently smooth or piecewise smooth. Then the discrete feature surface Γ_h carries additional information about Γ. Our surface reconstruction method is described in the next section.

3 Piecewise Quadratic Extrapolation of Piecewise Linear Surfaces

In this section, we consider again the feature surface Γ. To simplify the presentation, we assume that Θ is its boundary. We assume also that nodes of Γ_h and Θ_h belong to Γ and Θ, respectively, although this assumption is not necessary in practice.

The piecewise quadratic extrapolation $\tilde{\Gamma}_h$ of Γ_h is defined as the continuous surface being the closure of a union of open non-overlapping pieces $\tilde{\Gamma}_t$ of local quadratic extrapolations over faces Γ_t.

The local extrapolation $\tilde{\Gamma}_t$ is described by a quadratic function $\varphi_{2,t}$. Hereafter, we shall omit the superscript t whenever it does not result in confusion. For our purposes, it will be convenient to describe the function φ_2 in a local coordinate system (ξ_1, ξ_2) associated with the plane of Γ_t. In this coordinate system, the 2D multi-point Taylor formula [CI71] for a quadratic function φ_2 with the Hessian $H^{\varphi_2} = \{H^{\varphi_2}_{pq}\}^2_{p,q=1}$ reads

$$\varphi_2(\boldsymbol{\xi}) = -\frac{1}{2}\sum_{i=1}^{3}(H^{\varphi_2}(\boldsymbol{\xi} - \mathbf{a}_i),\, (\boldsymbol{\xi} - \mathbf{a}_i))\, p_i(\boldsymbol{\xi}) \tag{5}$$

where $\mathbf{a}_1, \mathbf{a}_2, \mathbf{a}_3$ are vertices of the triangle Γ_t and $p_i(\boldsymbol{\xi})$ is a piecewise linear function such that $p_i(\mathbf{a}_j) = \delta_{ij}$.

In order to recover the Hessian H^{φ_2}, we *first* assume that numbers $\alpha_i = (H^{\varphi_2}\ell_i,\, \ell_i)$, $i = 1, 2, 3$, representing the projection of this Hessian on edges ℓ_i of Γ_t, are given. Hereafter, we use ℓ_i for both the mesh edge and the corresponding vector. In the local coordinate system, vectors ℓ_i are described by two coordinates, $\ell_i = (l^i_1,\, l^i_2)$. We assume that the vector ℓ_i begins at vertex $\mathbf{a}_i$ and ends at vertex $\mathbf{a}_{i+1}$ with $\mathbf{a}_4 = \mathbf{a}_1$. Then, the definition of α_i gives

$$(\begin{pmatrix} H^{\varphi_2}_{11} & H^{\varphi_2}_{12} \\ H^{\varphi_2}_{12} & H^{\varphi_2}_{22} \end{pmatrix} \begin{pmatrix} l^i_1 \\ l^i_2 \end{pmatrix}, \begin{pmatrix} l^i_1 \\ l^i_2 \end{pmatrix}) = \alpha_i$$

which in turn results in the system of three linear equations for the unknown entries of the matrix H^{φ_2}:

$$l^i_1 l^i_1 H^{\varphi_2}_{11} + l^i_2 l^i_2 H^{\varphi_2}_{22} + 2\, l^i_1 l^i_2 H^{\varphi_2}_{12} = \alpha_i,\ i = 1, 2, 3. \tag{6}$$

Lemma 1. *The matrix of the system (6) is non-singular.*

Proof. Let us denote the coefficient matrix of system (6) by B. Note that $\ell_1 + \ell_2 + \ell_3 = 0$. Using this fact in direct calculations of the determinant of matrix B, we get

$$|\det B| = 2|l^1_1 l^2_2 - l^2_1 l^1_2|^3 = 16|\Gamma_t|^3 > 0 \tag{7}$$

where $|\Gamma_t|$ is the area of the triangle Γ_t. This proves the assertion of the lemma. □

Second, we use results of [AG99] where the algorithm for computing the discrete Hessian $H^h(\mathbf{a}_i)$ of a continuous piecewise linear function is presented and analyzed. We define α_i as the average of two nodal approximations,

$$\alpha_i = ((H^h(\mathbf{a}_i)\ell_i,\, \ell_i) + (H^h(\mathbf{a}_{i+1})\ell_i,\, \ell_i))/2, \tag{8}$$

associated with the edge ℓ_i. There are two exceptions from this rule. If $\mathbf{a}_i \in \Theta_h$ and $\mathbf{a}_{i+1} \notin \Theta_h$, then α_i is equal to $(H^h(\mathbf{a}_{i+1})\ell_i,\, \ell_i)$. If $\mathbf{a}_i \in \Theta_h$ and $\mathbf{a}_{i+1} \in \Theta_h$, then $\alpha_i = 0$. This implies that the nodal approximation of the Hessian is not recovered at feature edges and therefore the traces of Γ_h and $\tilde{\Gamma}_h$ on Θ_h coincide.

It remains to describe how we recover $H^h(\mathbf{a}_i)$ for every interior node $\mathbf{a}_i$ of Γ_h. We begin by introducing a few additional notations. For each $\mathbf{a}_i$, we define the superelement σ_i as a union of all triangles of Γ_h sharing $\mathbf{a}_i$. Then, we define a plane

approximating in the least square sense the nodes of this superelement and associate this plane with a local coordinate system (ξ_1, ξ_2). Let $\hat{\sigma}_i$ be the projection of σ_i onto the $\xi_1\xi_2$-plane. Further, let $\varphi(\xi_1, \xi_2)$ be the continuous function representing locally Γ, and $\varphi_h^i(\xi_1, \xi_2)$ be the continuous piecewise linear function representing σ_i. We assume that both functions are single-valued over $\hat{\sigma}_i$. Finally, we denote the Hessian of φ by H^φ.

The components H^h_{pq}, $p, q = 1, 2$, of the discrete Hessian H^h are defined in a weak sense by

$$\int_{\hat{\sigma}_i} H^h_{pq}(\mathbf{a}_i)\psi_h \,\mathrm{d}S = -\int_{\hat{\sigma}_i} \frac{\partial \varphi_h^i}{\partial \xi_p}\frac{\partial \psi_h}{\partial \xi_q}\,\mathrm{d}S, \tag{9}$$

which holds for any continuous piecewise linear function ψ_h vanishing on $\partial\hat{\sigma}_i$. Note that the discrete Hessian $H^h(\mathbf{a}_i)$ is a geometric characteristic of the feature surface Γ at point $\mathbf{a}_i$ (related to its curvature) and therefore is invariant of the position of the projection plane associated with the superelement σ_i. In other words, the value $(H^h(\mathbf{a}_i)\ell_i, \ell_i)$ is independent of the local transformation of the coordinate system.

In addition to the above invariance and the obvious uniqueness of H^h, the presented extrapolation is exact for quadratic surfaces as long as the triangle Γ_t has no edges on Θ_h. Indeed, for a quadratic function φ, the recovery method (9) is exact, i.e. $H^h_{pq}(\mathbf{a}_i) = H^\varphi_{pq}(\mathbf{a}_i)$. Therefore, for all $\mathbf{a}_i \notin \Theta_h$,

$$(H^\varphi \ell, \ell) = (H^h(\mathbf{a}_i)\ell, \ell)$$

for every edge $\ell \subset \Gamma_h \setminus \Theta_h$ and $H^{\varphi_2} = H^\varphi$ follows from (8) and Lemma 1.

The proposed reconstruction method is local and therefore it can be easily parallelized. Its computational cost is proportional to the number of surface triangles. It is pertinent to note that this cost is negligent compared to the cost of anisotropic mesh adaptation.

Now we consider the approximation property of our extrapolation method. For every triangle Γ_t, we define a superelement σ^t as union of superelements σ_i corresponding to vertices $\mathbf{a}_i$ of Γ_t. Again, we use the local coordinate system (ξ_1, ξ_2) associated with the triangle Γ_t. Let $\hat{\sigma}^t$ (resp., $\hat{\Gamma}_t$) be the projection of σ^t (resp., Γ_t) onto the $\xi_1\xi_2$-plane. We define the constant tensor $H^\varphi_{\sigma^t}$ for the superelement $\hat{\sigma}^t$ as

$$H^\varphi_{\sigma^t} = H^\varphi(\arg \max_{\boldsymbol{\xi}\in\hat{\sigma}^t} |det H^\varphi(\boldsymbol{\xi})|). \tag{10}$$

Theorem 1. *Let edges of a triangle Γ_t be interior edges of Γ_h and $\hat{\sigma}_t$ be a quasi-uniform triangulation with size h. Let $\varphi(\xi_1, \xi_2)$ be a $C^2(\hat{\sigma}^t)$ function representing locally Γ and $\varphi_h = \mathcal{I}_{\hat{\sigma}^t}\varphi$ be a continuous piecewise linear function representing σ^t. Moreover, let H^φ and H^h be the differential and discrete Hessians of φ and φ_h, respectively, such that*

$$\|H^\varphi_{pq} - H^\varphi_{\sigma^t,pq}\|_{L_\infty(\hat{\sigma}^t)} < \delta, \tag{11}$$

$$\|\nabla(\varphi - \mathcal{I}_{\hat{\sigma}^t}\varphi)\|_{L_2(\hat{\sigma}^t)} < \epsilon. \tag{12}$$

Then, the quadratic function φ_2 describing $\tilde{\Gamma}_t$ and defined by (5), (6), (8) and (9) satisfies

$$\|\varphi - \varphi_2\|_{L_\infty(\hat{\Gamma}_t)} \leqslant C(\epsilon + \delta h^2) \tag{13}$$

where constant C is independent of δ, ϵ, h and φ.

Proof. Hereinafter, we shall use C and C_i for generic constants having different values in different places. The definition (9) of the discrete Hessian implies that

$$\int_{\hat{\sigma}_i} (H^{\varphi}_{pq} - H^h_{pq}(\mathbf{a}_i))\psi_h \,\mathrm{d}S = -\int_{\hat{\sigma}_i} \frac{\partial(\varphi-\varphi_h)}{\partial\xi_p}\frac{\partial\psi_h}{\partial\xi_q}\,\mathrm{d}S$$

for any $\psi_h \in P_1(\hat{\sigma}_i)$ vanishing on $\partial\hat{\sigma}_i$. Now, using the triangle inequality and then the Cauchy inequality, we get

$$\begin{aligned}\int_{\hat{\sigma}_i} |H^{\varphi}_{\sigma^t,pq} - H^h_{pq}(\mathbf{a}_i)||\psi_h|\,\mathrm{d}S \leqslant{}& \left\|\frac{\partial(\varphi-\varphi_h)}{\partial\xi_p}\right\|_{L_2(\hat{\sigma}_i)} \left\|\frac{\partial\psi_h}{\partial\xi_q}\right\|_{L_2(\hat{\sigma}_i)} \\ &+ \int_{\hat{\sigma}_i} |H^{\varphi}_{\sigma^t,pq} - H^{\varphi}_{pq}||\psi_h|\,\mathrm{d}S.\end{aligned}$$

Let us evaluate all terms in the above inequality for a particular choice of ψ_h such that $\psi_h(\mathbf{a}_i) = 1$. The term in the left hand side is estimated from below as follows:

$$\int_{\hat{\sigma}_i} |H^{\varphi}_{\sigma^t,pq} - H^h_{pq}(\mathbf{a}_i)||\psi_h|\,\mathrm{d}S \geqslant C_1|H^{\varphi}_{\sigma^t,pq} - H^h_{pq}(\mathbf{a}_i)|\,|\hat{\sigma}_i|.$$

The terms in the right hand side may be easily estimated from above using quasi-uniformity of $\hat{\sigma}^t$ and assumption (11):

$$\left\|\frac{\partial\psi_h}{\partial\xi_q}\right\|_{L_2(\hat{\sigma}_i)} \leqslant C_2, \qquad \int_{\hat{\sigma}_i} |H^{\varphi}_{\sigma^t,pq} - H^{\varphi}_{pq}||\psi_h|\,\mathrm{d}S \leqslant C_3\delta|\hat{\sigma}_i|.$$

Combining the above inequalities, we get

$$|H^{\varphi}_{\sigma^t,pq} - H^h_{pq}(\mathbf{a}_i)| \leqslant \frac{C_2}{C_1|\hat{\sigma}_i|}\epsilon + \frac{C_3}{C_1}\delta. \tag{14}$$

Let H^{φ_2} be the Hessian of the quadratic function φ_2. The next step in the proof is to estimate the discrepancy between $H^{\varphi}_{\sigma^t}$ and H^{φ_2}. For this purpose, we use the perturbation analysis and Lemma 1. Since both Hessians $H^{\varphi}_{\sigma^t}$ and H^{φ_2} are constant, they are uniquely defined by the right hand side of system (6) and edges of triangle Γ_t. Let α_1, α_2 and α_3 be the entries of the right hand side, $H^{\varphi_2}_{pq}$ be the solution of (6), and let $\beta_i = (H^{\varphi}_{\sigma^t}\ell_i,\, \ell_i)$, $i = 1, 2, 3$. Using definition (8), inequality (14), a linear algebra estimate for eigenvalues of a 2×2 matrix, and the assumption of quasi-uniformity of $\hat{\sigma}^t$, we get

$$\begin{aligned}|\alpha_i - \beta_i| &= \frac{1}{2}|(H^h(\mathbf{a}_i)\ell_i,\, \ell_i) + (H^h(\mathbf{a}_{i+1})\ell_i,\, \ell_i) - 2(H^{\varphi}_{\sigma^t}\ell_i,\, \ell_i)| \\ &\leqslant 2\left(\frac{C_2\epsilon}{C_1 \min\limits_{i=1,2,3}|\hat{\sigma}_i|} + \frac{C_3}{C_1}\delta\right)(\ell_i,\, \ell_i) \leqslant C(\epsilon + \delta h^2).\end{aligned}$$

The perturbation analysis states that

$$|H^{\varphi_2}_{pq} - H^{\varphi}_{\sigma^t,pq}| \leqslant C\,|\lambda^{-1}_{\min}(B)| \max_{i=1,2,3}|\alpha_i - \beta_i|$$

where the matrix B is defined in Lemma 1 and $\lambda_{\min}(B)$ is its closest to zero eigenvalue. The application of the Gershgorin theorem and the quasi-uniformity assumption give the estimate for the maximal eigenvalue of B:

$$\lambda_{\max}(B) \leqslant 2 \max_{1 \leqslant i \leqslant 3} |\ell_i|^2 \leqslant Ch^2.$$

Therefore, due to (7)

$$|\lambda_{\min}(B)| \geqslant \frac{|\det B|}{\lambda^2_{\max}(B)} = \frac{16|\Gamma_t|^3}{\lambda^2_{\max}(B)} \geqslant Ch^2.$$

Using the last estimate, we get easily that

$$|H^{\varphi_2}_{pq} - H^{\varphi}_{\sigma^t,pq}| \leqslant C(\epsilon/h^2 + \delta). \tag{15}$$

Finally, by virtue of the multi-point Taylor formula for a general function φ whose linear interpolant φ_h vanishes on the triangle $\hat{\Gamma}_t = \Gamma_t$, we have:

$$\varphi(\boldsymbol{\xi}) = -\frac{1}{2}\sum_{i=1}^{3}(H^{\varphi}(\boldsymbol{\xi}^*_i)(\boldsymbol{\xi} - \mathbf{a}_i),\, (\boldsymbol{\xi} - \mathbf{a}_i))\, p_i(\boldsymbol{\xi})$$

where $\boldsymbol{\xi}^*_i(\boldsymbol{\xi})$ is a point inside $\hat{\Gamma}_t$, $\boldsymbol{\xi} \in \Gamma_t$. Together with formula (5), it gives

$$\begin{aligned} |\varphi(\boldsymbol{\xi}) - \varphi_2(\boldsymbol{\xi})| &= \frac{1}{2}\left|\sum_{i=1}^{3}([H^{\varphi}(\boldsymbol{\xi}^*_i) - H^{\varphi_2}](\boldsymbol{\xi} - \mathbf{a}_i),\, (\boldsymbol{\xi} - \mathbf{a}_i))\, p_i(\boldsymbol{\xi})\right| \\ &\leqslant C(\epsilon + \delta h^2). \end{aligned}$$

This proves the assertion of the theorem. □

Generally speaking, the values of ϵ and δ depend on the derivatives of φ. If φ is sufficiently smooth, for example it is in $C^3(\hat{\sigma}^t)$, then $\epsilon \sim h^3$ [CI78], $\delta \sim h$ and we get the expected result

$$\|\varphi - \varphi_2\|_{L_\infty(\hat{\Gamma}_t)} \leqslant Ch^3.$$

4 Numerical Experiments

As the model problem, we consider the convection-diffusion equation

$$\begin{aligned} -0.01\Delta u + \mathbf{b}\cdot\nabla u = 0 \quad &\text{in} \quad \Omega \\ u = g \quad &\text{on} \quad \Gamma_{in} \\ \frac{\partial u}{\partial n} = 0 \quad &\text{on} \quad \Gamma_{out} \\ u = 0 \quad &\text{on} \quad \partial\Omega \setminus (\Gamma_{in} \cup \Gamma_{out}). \end{aligned} \tag{16}$$

Here $\mathbf{b} = (1,0,0)^T$ is the velocity field, $\Omega = (0,1)^3 \setminus B_{0.5}(0.18)$ is the computational domain with $B_{0.5}(r) = \{\mathbf{x}\colon\ \sum_{i=1}^{3}(x_i - 0.5)^2 \leqslant r^2\}$, $\Gamma_{in} = \{\mathbf{x} \in \partial\Omega\colon\ x_1 = 0\}$, $\Gamma_{out} = \{\mathbf{x} \in \partial\Omega\colon\ x_1 = 1\}$, and $g(x_2, x_3) = 16x_2(1-x_2)x_3(1-x_3)$ is the standard Poiseille profile of the entering flow.

The solution u to (16) possesses a boundary layer along the upwind side of the spherical obstacle $B_{0.5}(0.18)$ and is very smooth in the shadow region of this obstacle. Since the exact solution is not known, in our experiments, we replace it with the piecewise linear finite element solution u_* computed on a very fine adaptive (quasi-optimal) mesh containing more than 1.28 million tetrahedra (see Fig. 2, left

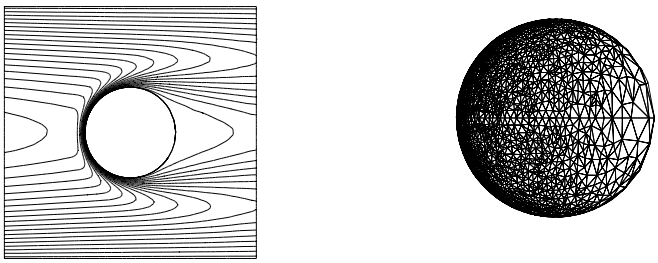

Fig. 2. Isolines of solution u_* in the plane passing through the center of the obstacle and parallel to the x_1x_2-plane (left picture) and the trace of a typical quasi-optimal mesh at the obstacle with analytic boundary (right picture)

picture). To built the adaptive mesh, we used the analytical representation of $\partial\Omega$. The trace of the adapted mesh on the surface of the obstacle shows coarsening in the shadow region and refinement in the upwind region (see Fig. 2, right picture).

In the first set of experiments (the top-left picture in Fig. 3), we demonstrate the asymptotic result (4) with u_* instead of u. The L_∞ error fits the analytic curve $60\,N(\Omega_h)^{-2/3}$.

In the second set of experiments (the top-right picture in Fig. 3), the boundary $\Gamma = \partial B_{0.5}(0.18)$ is approximated with a quasi-uniform mesh Γ_h. We measure the L_∞ error as a function of $N(\Omega_h)$ for three different values of h. Figure 3 presents saturation of this error due to the limited boundary resolution. We observe that the saturated error ε_h is almost reciprocal to h^2: $\varepsilon_{0.05} = 0.20$, $\varepsilon_{0.025} = 0.067$, and $\varepsilon_{0.0125} = 0.021$. This is probably related to the second order approximation of the smooth boundary Γ by the piecewise linear manifold Γ_h.

In these experiments, we fixed the nodes on Γ_h. The fixed-node constraints result in unnecessary fine mesh only in the shadow region of the obstacle (see Fig. 4, right picture). Therefore, the mesh is too stretched there in contract to the case of analytical representation of the obstacle boundary (see Fig. 4, left picture, and Fig. 2 for the mesh trace). This results in mesh elements with a lower quality in the shadow region. However, the excessive refinement and the low quality of these elements do not affect the value of the saturated error. The number of extra elements is small compared to $N(\Omega_h)$ and the solution is very smooth in these elements.

In the third set of experiments, we study the effect of the piecewise quadratic extrapolation $\tilde{\Gamma}_h$ of Γ_h on accuracy of the discrete solution. We compare saturation errors for three surface meshes: $\Gamma_{0.025}$, $\Gamma_{0.0125}$ and $\Gamma^*_{0.0125}$. The third mesh is obtained from $\Gamma_{0.0125}$ by projection its mesh nodes onto $\tilde{\Gamma}_{0.025}$. This mesh must provide the saturation error ε^*_h which is between saturation errors on the other two meshes. This is illustrated in the bottom picture of Fig. 3 where $\varepsilon_{0.0125} = 0.021$, $\varepsilon_{0.025} = 0.067$, and $\varepsilon^*_{0.0125} = 0.043$.

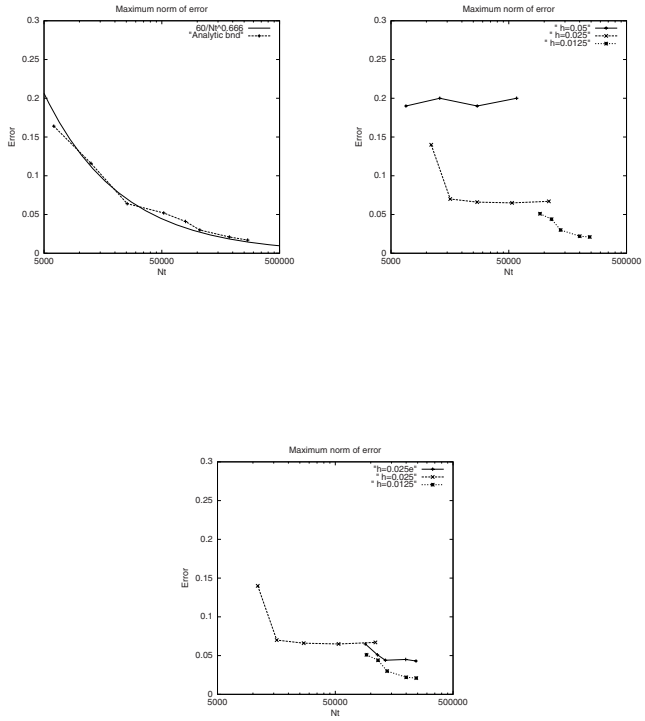

Fig. 3. Convergence analysis: using analytic representation of the obstacle boundary (top-left picture), using three discrete models $\Gamma_{0.05}$, $\Gamma_{0.025}$, and $\Gamma_{0.0125}$ for $\partial B_{0.5}(0.18)$ (top-right picture), using the piecewise quadratic extrapolation $\tilde{\Gamma}_{0.025}$ (bottom picture)

Another approach for building a piecewise linear surface $\Gamma^*_{0.0125}$ is based on the uniform refinement of $\Gamma_{0.025}$ with subsequent projection of new mesh nodes onto $\tilde{\Gamma}_{0.025}$. We use the first approach because it gives the most rigorous comparison of saturation errors on meshes $\Gamma_{0.0125}$ and $\Gamma^*_{0.0125}$.

In practice, the surface reconstruction should be dynamic and driven by the size of mesh elements. For the convection-diffusion problem (16), the surface extrapolation is required only in the upwind part of the obstacle boundary. We shall address this problem in the future.

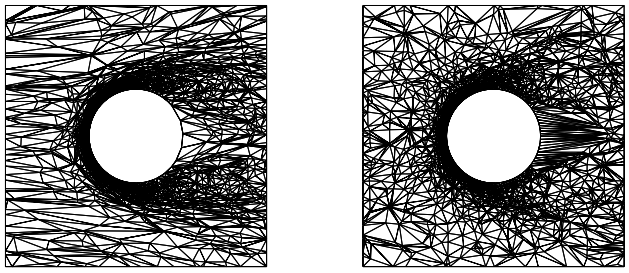

Fig. 4. The mesh cuts in the plane passing through the center of the obstacle and parallel to the x_1x_2-plane: The left picture corresponds to the case of analytic boundary representation. The right picture corresponds to the case of fixed-node constraints. The meshes have approximately the same number of elements ($\sim 200k$)

5 Conclusion

We have shown that representation of curved surfaces with triangular meshes restricts the use of adaptive methods. For a particular convection-diffusion problem, we have shown numerically that the saturated discretization error is proportional to h^2 where h is the size of the quasi-uniform mesh approximating the curved surface. We have proposed and analyzed theoretically and numerically a new surface reconstruction technique which improves performance of adaptive methods.

Acknowledgments. The work of the second author has been supported by the RFBR grant 04-07-90336 and the academic program "Computational and informatic issues of the solution of large problems".

[AG99] Agouzal A, Lipnikov K, Vassilevski Y (1999) East-West J Numer Math 7:223–244

[BO03] Bonnans JF, Gilbert C, Lemarécha C, Sagastizábal CA (2003) Numerical Optimization. Theoretical and Practical Aspects. Springer-Verlag, Berlin

[HE98] Borouchaki H, Hecht F, Frey PJ (1998) Inter J Numer Meth Engrg 43:1143–1165

[BU97] Buscaglia GC, Dari EA (1997) Inter J Numer Meth Engrg 40:4119–4136

[CI71] Ciarlet PG, Wagschal C (1971) Numer Math 17:84–100

[CI78] Ciarlet PG (1978) The finite element method for elliptic problems. North-Holland

[HA95] Dompierre J, Vallet M-G, Fortin M, Habashi WG, Ait-Ali-Yahia D, Tam A (1995) CERCA Report R95-73

[GA05] Garimella RV, Swartz BK (2003) Los Alamos Report LA-UR-03-8240

[GA04] Garimella R, Knupp P, Shashkov M (2004) Comput Meth Appl Mech Engng 193:913–928
[LI03] Lipnikov K, Vassilevski Y (2003) Comput Meth Appl Mech Engrg 192:1495–1513
[MI97] McIvor AM, Valkenburg RJ (1997) Machine Vision and Applications 10:17–26
[ME02] Meyer M, Lee H, Barr AH, Desbrun M (2002) Journal of Graphics Tools 7:13–22
[MO01] Mokhtarian F, Khalili N, Yuen P (2001) Computer Vision and Image Understanding 83:118–139
[NO99] Nocedal J, Wright SJ (1999) Numerical Optimization. Springer-Verlag, New York
[PE02] Petitjean S (2002) ACM Computing Surveys 32:211–262
[VA03] Vassilevski Y, Lipnikov K (2003) Comp Math Math Phys 43:827–835
[VA05] Vassilevski Y, Dyadechko V, Lipnikov K (2005) Russian J Numer Anal Math Modelling (to appear)